Latin American Journal of Solids and Structures
www.lajss.org

Theoretical Analysis of Stress Distribution in Bonded Single Strap and Stiffened Joints

Abstract

In this paper, distribution of peeling stress in two types of adhesively-bonded joints is investigated. The joints are a single strap and a stiffened joint. Theses joints are under uniform tensile load and materials are assumed orthotropic. Layers can be identical or different in mechanical or geometrical properties. A two-dimensional elasticity theory that includes the complete stress-strain and the complete strain-displacement relations for adhesive and adherends is used in this analysis. The displacement is assumed to be linear in the adhesive layer. A set of differential equations was derived and solved by using appropriate boundary conditions. Results revealed that the peak peeling stress developed within the adhesive layer is a function of geometrical and mechanical properties. FEM solution is used as the second method to verify the analytical results. A good agreement is observed between analytical and FEM solutions.

Keywords

Stress distribution, adhesive joint, strap joint, stiffened joint, finite element, peeling stress

Behnam Ghoddous [a]

[a] Young Researchers and Elite Club, Ahvaz branch, Islamic Azad University, Ahvaz, Iran, b.ghoddous@iauahvaz.ac.ir

http://dx.doi.org/10.1590/1679-78253147

Received 05.06.2016
In revised form 11.11.2016
Accepted 16.11.2016
Available online 29.11.2016

1 INTRODUCTION

Adhesively-bonded joints are widely used due to their several advantages over the other methods. Wider contact region in adhesively-bonded joints is the cause of more uniform stress distribution. In the same weight, bonded joints show more strength than the other common methods such as threaded connections, welding and riveting. Adhesively-bonded joints are stronger in fatigue, failure and they are corrosion resistant. Composite materials that are widely used these days are weak in local stresses so it is critical to use mechanical joints due to their stress concentration. Adhesively-bonding acts over areas not a single point so they are the best choice in bonding different composite layers. There are several joint designs for bonding the layers such as single-lap, double-lap, single strap, stepped-lap, stiffened, scarf butt, etc.

A number of studies have been conducted to analyze the stress distribution theoretically and numerically within the overlap length of adhesive layer. Ojalvo and Edinoff (1987), investigated the effects of thickness of a single-lap joint under tension. They assumed peeling stress to be constant along the thickness. Their work showed that the peak shear stress occurs at the both ends of the overlap region. Hart-Smith (1973), derived the iterative closed-form analytical solutions for single-lap adhesive joint which accounted for adhesive plasticity and adherend stiffness imbalance. Three distinct effects, bending due to eccentric loads, shear and peeling stress were covered in his analysis. He also studied a double-lap joint and showed that the effects of peeling stress are more pronounces in single-lap joints due to eccentric load path. Chuan her (1999), presented simplified one-dimensional models for single and double lap joints based on classical elasticity theory. He assumed shear deformation constant across the adhesive thickness. Shahin and Taheri (2009), presented analytical treatment of the deformations in adhesively-bonded joints on elastic foundation with special attention to the specific case of adhesive joint between the face sheets of sandwich beams. They studied single-lap, stiffened and single strap joints using strain energy method. They applied cylindrical bending theory to determine some coefficients to calculate moments on edges. Lou and Tong (2008), presented a novel formulation and analytical solutions for adhesively-bonded composite single-lap joint by taking into account the transvers shear deformation and large deflection in adherends. On the basis of geometrically nonlinear analysis for infinitesimal elements of adherends and adhesive, the equilibrium equations of adherends are formulated. They used Timoshenko beam theory to express the governing differential equations in terms of the adherend displacements. Their obtained solutions are applied to single-lap joints, whose adherends can be isotropic or composite laminates with symmetrically ups. They determined a new formula for adhesive peeling stress. Li et. Al. (1999), performed a nonlinear two-dimensional finite element analysis to determine the stress and strain distribution across the adhesive thickness of composite single lap joints. They showed that the tensile peeling and shear stresses at the bond free edges change significantly across the adhesive thickness. Vable et al. (2006), used boundary element method to study stress gradient in adhesively bonded joints. Their work included both single- and double-lap joints. Numerical results of single- and double-lap joints showed the potential of boundary element method in analysis of bonded joints. Zhao and Lu (2009), developed a general two-dimensional analytical approach capable of providing an explicit closed-form solution for the calculation of elastic stresses in single-lap joint, Assuming linear distribution of a longitudinal normal stress in the joint thickness direction. By treating the adhesive layer in the same way as the adherends, the two-dimensional stress and strain distributions at any point, and the tensile force, shearing and bending moment at any cross section can be predicted accurately, in both the adhesive and adherends. Their analysis was based on a two-dimensional elasticity theory that both includes the complete stress-strain and the complete strain-displacement relationships for the adhesive and adherends. Their method was capable of satisfying all the boundary stress conditions of the joint, including the stress-free surface condition at the ends of the bondline. Sawa et. al. (2000), analyzed single-lap adhesive joints of dissimilar adherends subjected to tensile loads as a three body contact problem using two dimensional theory of elasticity. They examined the effects of Young's modulus ratio between different adherends thickness, the ratio of the adherends length and the adhesive thickness on contact stress distributions at the interfaces. Temiz et. al. (2015), used FEM to analyze behavior of bi-adhesive used in

repairing of damaged parts. In a double-strap joint with an embedded patch, patch was embedded into the adherents for structural requirements. In addition, to increase the strength of the joint, two adhesives were used to bond the adherends. They used nonlinear finite element method to predict the failure loads to assist with the geometric design and to identify effective ratios of sizes to maximize joint strength. Shishesaz and Bavi (2012) had an investigation on void and debond effects in a double lap joint. For symmetric debonds and voids with relative lengths of 0.8, the same effects were observed. In a comparison for defects between single-lap and double-lap joints they reported that the increase in stress is higher in single-lap joint than in double lap joints. Karachalios et al. (2013), studied the effect of defects on the strength of a single-lap joint with various adherend and adhesive materials. Two different types of adhesive were studied with different degrees of ductility since the stress distribution along the overlap depends on the adhesive's capacity to deform plastically. Steel adherends were used from low strength and high ductility to high strength. Rectangular and circular defects located in the middle of the overlap were studied. The artificial defect consists of a thin film of Teflon placed in the middle of the overlap, thus creating a disbond of the required size. When a toughened structural adhesive is used with a high-strength steel, there is an almost linear decrease in joint strength as the defect area increases. In the case of the brittle adhesive, the reduction in strength, as the defect size increases, is not proportional for small defect sizes, indicating that the end of the joint becomes more important due to local strains exceeding limiting values. Ghoddous and shishehsaz (2016), investigated an adhesively-bonded stepped-lap joint suffering from a void within its adhesive layer. They used classical elasticity theory to determine shear stress field in the separated sections of the adhesive layer along the overlap length. They declared that the stepped-lap joint performed better in stress distribution with void rather than single-lap and double-lap joint.

In this paper, peeling and shear stress distribution in the middle of the adhesive layer and peeling stress field between adhesive and adherends in a single strap joint and a stiffened joint are studied. The adherends are orthotropic and it is assumed that the adherends have bending deformation beside longitudinal displacement. The adhesive layer shows shear defamation. Longitudinal and transversal displacement equations are considered as a linear function in the thickness direction. Shear stress is assumed to be constant across the adhesive layer and the layers can be either similar or dissimilar in geometry or mechanical properties. The analytical solution can satisfy the boundary conditions completely. Theoretical results are verified by FEM results which obtained from ANSYS software.

2 ANALYTICAL SOLUTION

2.1 Stiffened Joint

In a stiffened joint, an extra layer as a doubler is bonded to the primary layers and improves the strength of the joint. The layer causes moment in the joint and shear and normal stresses in the adhesive and adherends layer. The external tensile load is inline and there is no eccentric load. The joint is consisted of two composite layers with orthotropic structures. Mechanical and geometrical properties of theses layers such as thickness, Young's modulus and Poisson's ratio can be different.

The model of the joint can be reduced to a two-dimensional model because the load is uniform and shear and normal stresses are not varied in the z direction. Figure 1 shows a model of the joint.

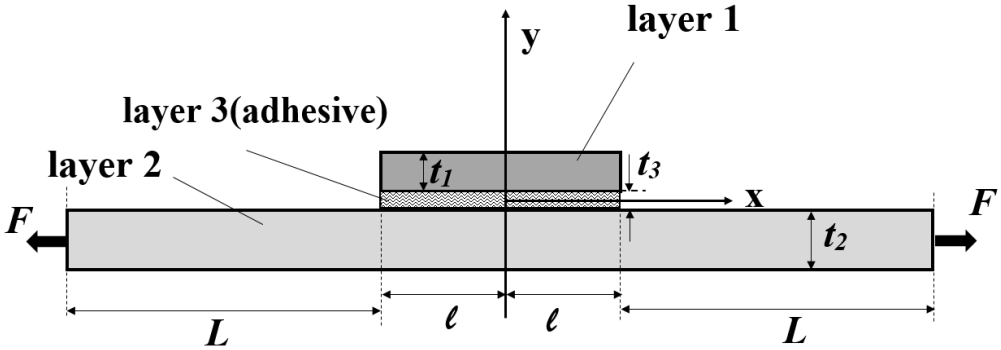

Figure 1: stiffened lap joint configuration.

E_{ix} and E_{iy} are the elastic modulus of the layers in x and y directions . μ_{ixz} and μ_{izx} are Poisson's ratio. f_1 and f_2 are internal forces in the unit of width in the layers 1 and 2 respectively. F is the external tensile force applied uniformly to the joint in x direction. The following assumptions are assumed in this analysis. The mode of this analysis is plain stress. It means that the stresses in z direction are constant. Shear stress is assumed to be constant through the adhesive layer. Differential equation of transversal and longitudinal displacements in the adhesive is assumed to be a linear function. Axial force is ignored in the adhesive layer due to the small Young's modulus of adhesive rather than the Young's modulus of adherends. Cylindrical bending theory is used to calculate deformations in the adhesive and adherends. Free body diagrams for an infinitesimal element in the overlap region are shown in Figure 2. τ_1, τ_2 are shear stresses and σ_{1y}, σ_{2y} are peel stresses in layer 1 and 2.

From the equilibrium in x and y direction:

$$\frac{df_1}{dx} + \tau_3 = 0 \tag{1-a}$$

$$\frac{df_2}{dx} - \tau_3 = 0 \tag{1-b}$$

$$\frac{dQ_1}{dx} + \sigma_{3y}^{u} = 0 \tag{2}$$

$$\frac{dQ_2}{dx} - \sigma_{3y}^{l} = 0 \tag{3}$$

$$\frac{d\tau_3}{dx}t_3-(\sigma_{3y}^{u}-\sigma_{3y}^{l})=0 \tag{4}$$

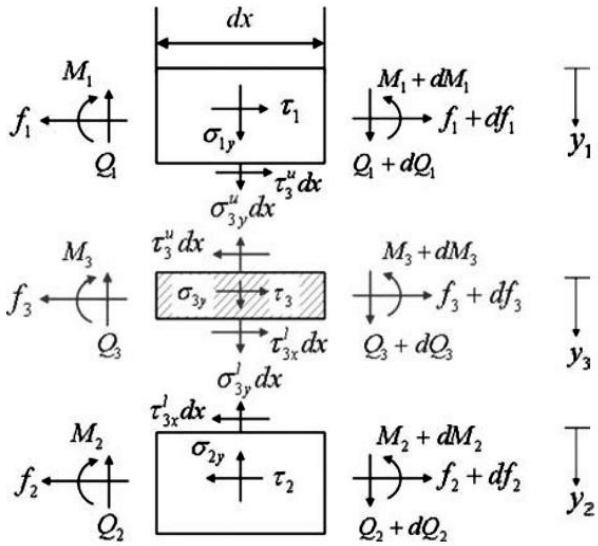

Figure 2: Free-body stress equilibrium diagram.

From the moment equilibrium in layer 1 and 2:

$$\frac{dM_1}{dx}-Q_1+\tau_3\frac{t_1}{2}=0 \tag{5-a}$$

$$\frac{dM_2}{dx}-Q_2+\tau_3\frac{t_2}{2}=0 \tag{5-b}$$

$\tau_3=\tau_3(x)=\tau_m$ is the shear stress in adhesive. σ_{3y}^{u}, σ_{3y}^{l} are peel stress between adhesive and layer 1 and 2 respectively. The relationship between force and moment in the layers with axial stress in x direction is:

$$\sigma_{ix}=f_i/t_i+6M_i(2\rho_i-1)/t_i^2 \tag{6}$$

$$0\le y_i\le t_i,\ \rho_i=y_i/t_i \qquad (i=1,2) \tag{7}$$

From the elasticity theory and equilibrium:

$$\frac{\partial\sigma_{ix}}{\partial x}+\frac{\partial\tau_i}{\partial y_i}=0 \qquad (i=1,2,3) \tag{8-a}$$

$$\frac{\partial\sigma_{iy}}{\partial y_i}+\frac{\partial\tau_i}{\partial x}=0 \qquad (i=1,2,3) \tag{8-b}$$

The subscripts 1, 2 and 3 denote the upper adherend, lower adherend and adhesive, respectively. Substituting Equations 8-a, 8-b into 6 and using the Equations 1-a, 1-b, 2, 3 and 4:

$$\tau_1 = \tau_3(3\rho_1^2 - 2\rho_1) - 6Q_1(\rho_1^2 - \rho_1)/t_1 \tag{9-a}$$

$$\tau_2 = \tau_3(3\rho_2^2 - 4\rho_2 + 1) - 6Q_2(\rho_2^2 - \rho_2)/t_2 \tag{9-b}$$

Where,

$$\rho_1 = 0 \;\Rightarrow\; \tau_1 = 0 \tag{10-a}$$

$$\rho_2 = 1 \;\Rightarrow\; \tau_2 = 0 \tag{10-b}$$

Substituting Equations 9-a, 9-b into 8-a, 8-b:

$$\sigma_{1y} = \frac{d\tau_3}{dx} t_1(-\rho_1^3 + \rho_1^2) + \sigma_{3y}^u(-2\rho_1^3 + 3\rho_1^2) \tag{11-a}$$

$$\sigma_{2y} = \frac{d\tau_3}{dx} t_2(-\rho_2^3 + 2\rho_2^2 - \rho_2) + \sigma_{3y}^l(2\rho_2^3 - 3\rho_2^2 + 1) \tag{11-b}$$

$$\sigma_{3y} = \sigma_{3y}^u - \frac{d\tau_3}{dx} t_3(\rho_3 + 0.5) \tag{11-c}$$

Where,

$$-0.5 \le \rho_3 (= y_3/t_3) \le 0.5 \tag{12}$$

Constants of integrations for the Equations 11-a and 11-b are determined by Equation 10 and for the Equation 11-c, Equation 13 is used.

$$\rho_3 = -0.5 \;\Rightarrow\; \sigma_{3y} = \sigma_{3y}^u \tag{13}$$

picking $\rho_3 = 0$, and using the Equation 11-c lead to calculate peeling stress in the middle of adhesive layer σ_m . using Equation 11-c and picking $\rho_3 = -0.5$ and $\rho_3 = 0.5$:

$$\sigma_{3y}^u = \sigma_m + \frac{d\tau_m}{dx}\frac{t_3}{2} \tag{14-a}$$

$$\sigma_{3y}^l = \sigma_m - \frac{d\tau_m}{dx}\frac{t_3}{2} \tag{14-b}$$

Relationship between shear stress and shear modulus is shown in Equation 15.

$$\gamma_{ixy} = \frac{\tau_i}{G_i} \quad (i = 1,2,3) \tag{15}$$

Stress-strain relationship for orthotropic materials is depicted by Equation 16.

$$\begin{bmatrix} \sigma_{ix} \\ \sigma_{iy} \\ \tau_i \end{bmatrix} = \begin{bmatrix} \frac{E_{ix}}{D_i} & \frac{\mu_{ixz} E_{iy}}{D_i} & 0 \\ \frac{\mu_{ixz} E_{iy}}{D_i} & \frac{E_{iy}}{D_i} & 0 \\ 0 & 0 & G_i \end{bmatrix} \begin{bmatrix} \varepsilon_{ix} \\ \varepsilon_{iy} \\ \gamma_{ixy} \end{bmatrix} \quad (i = 1,2) \tag{16}$$

$$D_i = 1 - \mu_{ixz}\mu_{izx} \tag{17}$$

Peeling stress and strain is derived from Equation 16 as follow:

$$\sigma_{iy} = \frac{E_{iy}}{D_i}\frac{\partial v_i}{\partial y_i} + \frac{\mu_{ixz} E_{iy}}{D_i}\varepsilon_{ix} \quad (i = 1,2) \tag{18}$$

$$\varepsilon_{iy} = \frac{\partial v_i}{\partial y_i} = A_i \left(\mu_{ixz} E_{iy} \sigma_{ix} - E_{ix} \sigma_{iy} \right) \tag{19}$$

Where,

$$A_i = \frac{D_i}{E_{ix} E_{iy} - \mu_{ixz}^2 E_{iy}^2} \ (i = 1,2) \tag{20}$$

For transversal displacement of the layer 1, by substituting Equations 6 and 11-a into Equation 19 and then integrating by ρ_1:

$$\begin{aligned} v_1 = {} & v_{1u} + A_1 t_1 \int_0^{\rho_1} \left(\mu_{1xz} E_{1y} \sigma_{1x} - E_{1x} \sigma_{1y} \right) d\rho_1 = \\ & v_{1u} + A_1 t_1 E_{1x} \left[\frac{d\tau_3}{dx} t_1 \left(-\frac{\rho_1^4}{4} + \frac{\rho_1^3}{3} \right) + \sigma_{3y}^{\mu} \left(-\frac{\rho_1^4}{2} + \rho_1^3 \right) \right] - \\ & \mu_{1xz} A_1 E_{1x} \left[f_1 \rho_1 + \frac{6M_1}{t_1} (\rho_1^2 - \rho_1) \right] \end{aligned} \tag{21}$$

v_{1u} is the transversal displacement for top surface of the layer 1. Transversal displacement between adhesive and layer 1 is derived by continuity of displacement and using Equation 21 as follow:

$$v_{1l} = v_1(\rho_1 = 1) = v_{1u} + A_1 t_1 E_{1x} \left(\frac{d\tau_3}{dx} \frac{t_1}{12} + \frac{\sigma_{3y}^{\mu}}{2} \right) - \mu_{1xz} A_1 E_{1y} f_1 \tag{22}$$

By substituting Equation 22 into Equation 23:

$$v_1 = v_{1l} + A_1 t_1 E_{1x}\left[\frac{d\tau_3}{dx} t_1\left(-\frac{\rho_1^4}{4}+\frac{\rho_1^3}{3}-\frac{1}{12}\right)+\sigma_{3y}^u\left(-\frac{\rho_1^4}{2}+\rho_1^3-\frac{1}{2}\right)\right]- \mu_{1xz} A_1 E_{1y}\left[f_1(\rho_1-1)+\frac{6M_1}{t_1}(\rho_1^2-\rho_1)\right] \tag{23}$$

Similarly for the layer 2:

$$v_2 = v_{2u} + A_2 t_2 E_{2x}\left[\frac{d\tau_3}{dx} t_2\left(-\frac{\rho_2^4}{4}+\frac{2\rho_2^3}{3}-\frac{\rho_2^2}{2}\right)+\sigma_{3y}^l\left(\frac{\rho_1^4}{2}-\rho_2^3+\rho_2\right)\right]- \mu_{2xz} A_2 E_{2y}\left[f_2\rho_2+\frac{6M_2}{t_2}(\rho_2^2-\rho_2)\right] \tag{24}$$

From continuity of displacements:

$$\begin{aligned} v_{3u} &= v_{1l}\,,\ u_{3u} = u_{1l} \\ v_{3l} &= v_{2u}\,,\ u_{3l} = u_{2u} \end{aligned} \tag{25}$$

For longitudinal displacements:

$$\gamma_i = \frac{\partial u_i}{\partial y_i} + \frac{\partial v_i}{\partial x} \quad (i = 1,2,3) \tag{26}$$

By substituting Equation 23 into Equation 26, using Equation 15 and integrating by ρ_1:

$$\rho_1 = 1 \ \Rightarrow u_1 = u_{1l} \tag{27}$$

$$u_1(\rho_1) = u_{1l} - \frac{dv_{1l}}{dx} t_1(\rho_1-1) - Q_1\left(\frac{1}{G_1}-\mu_{1xz}A_1E_{1y}\right)(2\rho_1^3-3\rho_1^2+1)- A_1 t_1^2 E_{1x}\left[\frac{d^2\tau_3}{dx^2} t_1\left(-\frac{\rho_1^5}{20}+\frac{\rho_1^4}{12}-\frac{\rho_1}{12}+\frac{1}{20}\right)+\frac{d\sigma_{3y}^u}{dx}\left(-\frac{\rho_1^5}{10}+\frac{\rho_1^4}{4}-\frac{\rho_1}{2}+\frac{7}{20}\right)\right]+ \tau_3 t_1\left[\left(\frac{1}{G_1}-\mu_{1xz}A_1E_{1y}\right)\left(\rho_1^3-\rho_1^2\right)+\mu_{1xz}A_1E_{1y}(\rho_1-1)\right] \tag{28}$$

For the layer 2 similarly:

$$
\begin{aligned}
&u_2(\rho_2) = u_{2u} + \int_0^{\rho_2} (\gamma_2(\rho_2) - \frac{\partial v_2}{\partial x}) t_2 d\rho_2 = \\
&u_{2u} - Q_2 \left(\frac{1}{G_2} - \mu_{2xz} A_2 E_{2y} \right) (2\rho_2^3 - 3\rho_2^2) - \frac{dv_{2u}}{dx} t_2 \rho_2 - \\
&A_2 t_2^2 E_{2x} \left[\frac{d^2\tau_3}{dx^2} t_2 \left(-\frac{\rho_2^5}{20} + \frac{\rho_2^4}{6} - \frac{\rho_2^3}{6} \right) + \frac{d\,\sigma_{3y}^l}{dx} \left(\frac{\rho_2^5}{10} - \frac{\rho_2^4}{4} + \frac{\rho_2^2}{2} \right) \right] + \\
&\tau_3 t_2 \left[\left(\frac{1}{G_2} - \mu_{2xz} A_2 E_{2y} \right) \left(\rho_2^3 - 2\rho_2^2 + \rho_2 \right) + \mu_{2xz} A_2 E_{2y}\ \rho_2 \right]
\end{aligned}
\tag{29}
$$

u_{2u} is the displacement of top surface of layer 2 (bonded surface).

$$M_i = \int_0^1 \sigma_{ix} (\rho_i - 0.5) t_i^2 d\rho_i \tag{30}$$

$$f_i = \int_0^1 \sigma_{ix} t_i d\rho_i \tag{31}$$

Using Equations 11 and 16:

$$\sigma_{1x} = \mu_{1xz} \left(\frac{d\tau_3}{dx} t_1 (-\rho_1^3 + \rho_1^2) + \sigma_{3y}^u (-2\rho_1^3 + 3\rho_1^2) \right) + \frac{1}{A_1 E_{1y}} \left(\frac{\partial u_1}{\partial x} \right) \tag{32-a}$$

$$\sigma_{2x} = \mu_{2xz} \left(\frac{d\tau_3}{dx} t_2 (-\rho_2^3 + 2\rho_2^2 - \rho_2) + \sigma_{3y}^l (2\rho_2^3 - 3\rho_2^2 + 1) \right) + \frac{1}{A_2 E_{2y}} \left(\frac{\partial u_2}{\partial x} \right) \tag{32-b}$$

By substituting Equations 32 into Equations 30 and 31 and using Equations 1 to 4:

$$
\begin{aligned}
\frac{d^2 v_{1l}}{dx^2} = &\left(\frac{11 A_1 E_{1x} t_1^2}{210} \right) \frac{d^3\tau_3}{dx^3} + \left(\frac{6}{5} \mu_{1xz} A_1 E_{1y} - \frac{1}{10 G_1} \right) \frac{d\tau_3}{dx} + \\
&\left(\frac{13 A_1 E_{1x} t_1}{35} \right) \frac{d^2\sigma_{3y}^u}{dx^2} + \frac{12}{5 t_1} \left(\mu_{1xz} A_1 E_{1y} - \frac{1}{2 G_1} \right) \sigma_{3y}^u - \frac{12 M_1 A_1 E_{1y}}{t_1^3}
\end{aligned}
\tag{33-a}
$$

$$
\begin{aligned}
\frac{d^2 v_{2u}}{dx^2} = &\left(\frac{11 A_2 E_{2x} t_2^2}{210} \right) \frac{d^3\tau_3}{dx^3} + \left(\frac{6}{5} \mu_{2xz} A_2 E_{2y} - \frac{1}{10 G_2} \right) \frac{d\tau_3}{dx} - \\
&\left(\frac{13 A_2 E_{2x} t_2}{35} \right) \frac{d^2\sigma_{3y}^l}{dx^2} - \frac{12}{5 t_2} \left(\mu_{2xz} A_2 E_{2y} - \frac{1}{2 G_2} \right) \sigma_{3y}^l - \frac{12 M_2 A_2 E_{2y}}{t_2^3}
\end{aligned}
\tag{33-b}
$$

Similarly to Equations 33-a and 33-b:

$$\frac{du_{1l}}{dx}=-\frac{t_1^3A_1E_{1x}}{105}\frac{d^3\tau_3}{dx^3}-\left(\frac{4t_1\mu_{1xz}A_1E_{1y}}{15}-\frac{2t_1}{15G_1}\right)\frac{d\tau_3}{dx}+\frac{f_1A_1E_{1y}}{t_1}-\frac{11t_1^2A_1E_{1x}}{210}\frac{d^2\sigma_{3y}^u}{dx^2}-\left(\frac{6\mu_{1xz}A_1E_{1y}}{5}-\frac{1}{10G_1}\right)\sigma_{3y}^u+\frac{6M_1A_1E_{1y}}{t_1^2} \tag{34-a}$$

$$\frac{du_{2u}}{dx}=\frac{t_2^3A_2E_{2x}}{105}\frac{d^3\tau_3}{dx^3}+\left(\frac{4t_2\mu_{2xz}A_2E_{2y}}{15}-\frac{2t_2}{15G_2}\right)\frac{d\tau_3}{dx}+\frac{f_2A_2E_{2y}}{t_2}-\frac{11t_2^2A_2E_{2x}}{210}\frac{d^2\sigma_{3y}^l}{dx^2}-\left(\frac{6\mu_{2xz}A_2E_{2y}}{5}-\frac{1}{10G_2}\right)\sigma_{3y}^l-\frac{6M_2A_2E_{2y}}{t_2^2} \tag{34-b}$$

Differential equations of transversal and longitudinal displacement are assumed to be linear in the ρ_3 direction.

$$u_3=0.5(u_{2u}+u_{1l})+\rho_3(u_{2u}-u_{1l}) \tag{35-a}$$

$$v_3=0.5(v_{2u}+v_{1l})+\rho_3(v_{2u}-v_{1l}) \tag{35-b}$$

Where v_3 is transversal displacement and u_3 is longitudinal displacement in adhesive. Shear stress in the middle line of adhesive thickness τ_m is obtained by substituting Equations 35 in Equation 26 and derivation:

$$\tau_m=\tau_3(\rho_3=0)=G_3\left[\frac{(u_{2u}-u_{1l})}{t_3}+\frac{1}{2}\left(\frac{dv_{2u}}{dx}+\frac{dv_{1l}}{dx}\right)\right] \tag{36}$$

Neglecting axial load in adhesive layer (σ_{3x}), peeling stress in the middle layer of adhesive σ_m is derived in Equation 37.

$$\sigma_m=\sigma_{3y}(\rho_3=0)=E_3\frac{\partial v_3}{\partial y_3}=\frac{E_3}{t_3}(v_{2u}-v_{1l}) \tag{37}$$

Derivation of Equations 36 and 37, substituting Equations 33 and 34 and using 14-a and 14-b lead to elimination of σ_{3y}^u and σ_{3y}^l.

$$(\alpha_1D^3-\alpha_2D)\tau_m+(\alpha_7D^2-\alpha_8)\sigma_m=\frac{6A_1E_{1y}}{t_1^3}\left((t_1+t_3)M_1+\frac{t_1^2f_1}{6}\right)+\frac{6A_2E_{2y}}{t_2^3}\left((t_2+t_3)M_2-\frac{t_2^2f_2}{6}\right) \tag{38-a}$$

$$(\alpha_7 D^3 - \alpha_8 D)\tau_m + (\alpha_4 D^2 - \alpha_5)\sigma_m = \frac{12M_1 A_1 E_{1y}}{t_1^3} - \frac{12M_2 A_2 E_{2y}}{t_2^3} \tag{38-b}$$

Where D=d/dx and $\alpha_i (i = 1,2,...,11)$ is a simplifier coefficient and is related to geometrical and mechanical configurations of the adhesive and adherends.

Derivation of Equations 38-a and 38-b and substitution of derivation moment M_i and force f_i by using Equations 1 and 5 create nonhomogeneous differential Equations 39-a and 39-b

$$(\alpha_1 D^4 - \alpha_2 D^2 + \alpha_{10})\tau_m + (\alpha_7 D^3 - \alpha_8 D)\sigma_m = \frac{6(t_1 + t_3)Q_1 A_1 E_{1y}}{t_1^3} - \frac{6(t_2 + t_3)Q_2 A_2 E_{2y}}{t_2^3} \tag{39-a}$$

$$(\alpha_7 D^3 - \alpha_8 D + \alpha_{11})\tau_m + (\alpha_4 D^3 - \alpha_5 D)\sigma_m = \frac{12Q_1 A_1 E_{1y}}{t_1^3} - \frac{12Q_2 A_2 E_{2y}}{t_2^3} \tag{39-b}$$

Derivation of Equations 39-a and 39-b and using Equations 2, 3 and 14 to eliminate derivation of shear force dQ_i/dx create two fifth order linear homogeneous differential Equations.

$$(\alpha_1 D^5 - \alpha_2 D^3 + \alpha_3 D)\tau_m + (\alpha_7 D^4 - \alpha_8 D^2 + \alpha_9)\sigma_m = 0 \tag{40-a}$$

$$(\alpha_7 D^5 - \alpha_8 D^3 + \alpha_9 D)\tau_m + (\alpha_4 D^4 - \alpha_5 D^2 + \alpha_6)\sigma_m = 0 \tag{40-b}$$

Shear stress distribution and peel stress distribution can be found by solution of Equations 40-a and 40-b.

In this type of joint layer 2 is under tensile load and layer 1 isn't subjected. Thus,

$$\int_{-l}^{l} \tau_m dx = 0 \tag{41}$$

For the free surfaces of adhesive in its ends:

$$\tau_m \Big|_{x = \mp l} = 0 \tag{42}$$

Figure 3 shows edge loads in adhesive region.

For the boundary conditions of loads shown in figure 3:

$$x = -l \;\Rightarrow\; M_1 = Q_1 = f_1 = \tau_3 = 0, M_2 = M_1^*, Q_2 = Q_1^*, f_2 = F \tag{43-a}$$

$$x = l \;\Rightarrow\; M_2 = -M_2^*, Q_2 = Q_2^*, f_2 = F, M_1 = Q_1 = f_1 = \tau_3 = 0 \tag{43-b}$$

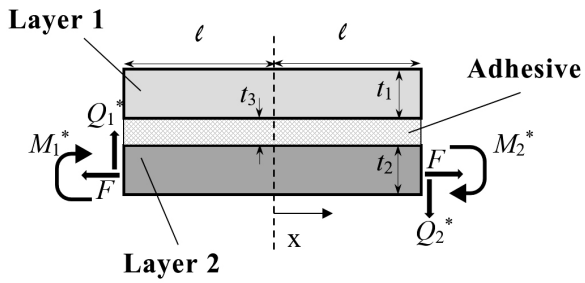

Figure 3: A section of adhesive and its edge loads in the stiffened joint.

Substituting Equations 43-a and 43-b into Equations 38-a, 38-b, 39-a and 39-b determines the other essential boundary conditions to solve Equations 40-a and 40-b. the edges load can be determined by calculating deformations in different parts of the joint. As the joint is symmetric, a half of it is shown in figure 4.

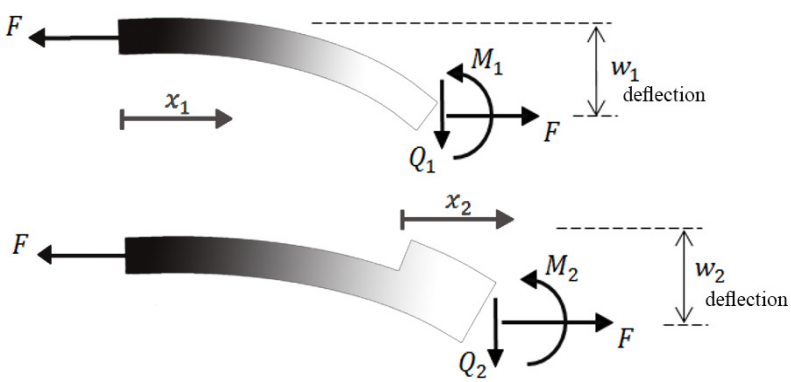

Figure 4: Deflections in different section of stiffened joint.

$$w_1 = C_1 \cosh \beta_1 x_1 + C_2 \sinh \beta_1 x_1 \tag{44-a}$$

$$w_2 = C_3 \cosh \beta_2 x_2 + C_4 \sinh \beta_2 x_2 + \eta \tag{44-b}$$

To determine the set of C coefficients four boundary conditions is needed.

$$x_1 = 0 : w_1 = 0 \tag{45-a}$$

$$x_1 = L_1, x_2 = 0 : w_1 = w_2 \tag{45-b}$$

$$x_1 = L_1, x_2 = 0 : \frac{dw_1}{dx_1} = \frac{dw_2}{dx_2} \tag{45-c}$$

$$x_2 = l : \frac{dw_2}{dx_2} = 0 \tag{45-d}$$

As the joint symmetric:

$$M_1^* = M_2^* = -D_{2u} \left. \frac{d^2 w_1}{dx_1^2} \right|_{x_1 = L} \tag{46}$$

2.2 Single Strap Joint

Single strap joint is consisted of three composite layer with orthotropic properties. It can be either symmetric or asymmetric in geometry and property. Figure 5 shows a two-dimensional model of a single strap joint.

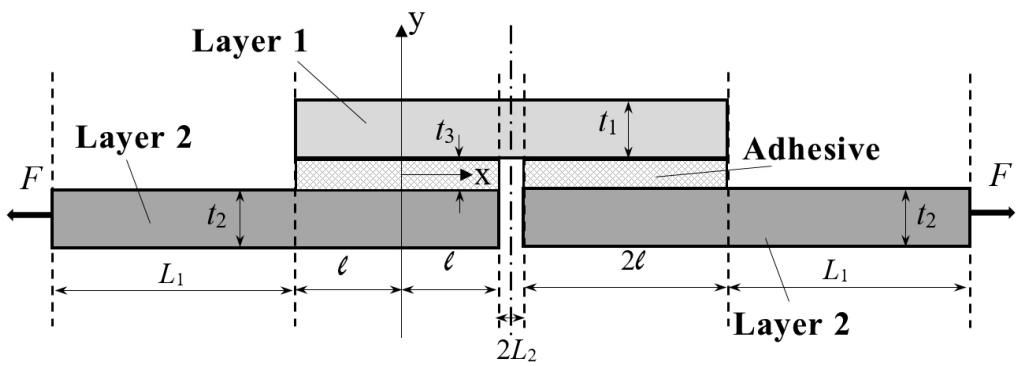

Figure 5: Single strap joint configuration.

Analytical solution of the joint is similar with the solution of previous joint and derived differential Equations expressed in Equations 40-a and 40-b are valid here. Figure 6 shows edge loads in three different sections. Set of Equations 47 expressed deflection function of adhesive and adherends.

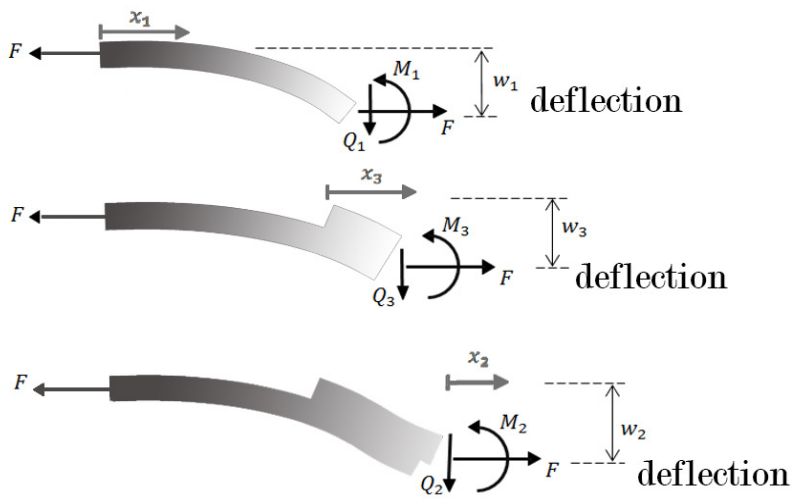

Figure 6: deflections in different section of single strap joint.

$$\frac{d^2w_1}{dx_1^2} = -\frac{M_1}{D_{1u}} = -\frac{F}{D_{1u}}(-w_1) \tag{47-a}$$

$$\frac{d^2w_2}{dx_2^2} = -\frac{M_2}{D_{2u}} = -\frac{F}{D_{2u}}\left[-w_2 - \frac{1}{2}(t_1+t_2)\right] \tag{47-b}$$

$$\frac{d^2w_3}{dx_3^2} = -\frac{M_3}{D_{3u}} = -\frac{F}{D_{3u}}\left[-w_3 - \frac{t_2}{2} + \eta\right] \tag{47-c}$$

General solution of Equations 47-a to 47-c is derived in set of Equation 48.

$$w_1 = C_1\cosh\beta_1 x_1 + C_2\sinh\beta_1 x_1 \tag{48-a}$$

$$w_2 = C_3\cosh\beta_2 x_2 + C_4\sinh\beta_2 x_2 - (t_1+t_2)/2 \tag{48-b}$$

$$w_3 = C_5\cosh\beta_3 x_3 + C_6\sinh\beta_3 x_3 + \eta \tag{48-c}$$

To determine the set of C coefficients six boundary conditions is needed.

$$x_1 = 0:\ w_1 = 0 \tag{49-a}$$

$$x_1 = L_1, x_3 = 0:\ w_1 = w_3 \tag{49-b}$$

$$x_1 = L_1, x_3 = 0:\ \frac{dw_1}{dx_1} = \frac{dw_3}{dx_3} \tag{49-c}$$

$$x_2 = 0, x_3 = 2l:\ \frac{dw_2}{dx_2} = \frac{dw_3}{dx_3} \tag{49-d}$$

$$x_2 = 0, x_3 = 2l:\ w_2 = w_3 \tag{49-e}$$

$$x_2 = L_2:\ \frac{dw_2}{dx_2} = 0 \tag{49-f}$$

Finally, determination of edge loads is done by using Equations 50-a to 50-d

$$M_1^* = -D_{1u}\left.\frac{d^2w_1}{dx_1^2}\right|_{x_1=L_1} \tag{50-a}$$

$$M_2^* = -D_{2u}\left.\frac{d^2w_2}{dx_2^2}\right|_{x_2=0} \tag{50-b}$$

$$Q_1^* = D_{1u}\left.\frac{d^3w_1}{dx_1^3}\right|_{x_1=L_1} \tag{50-c}$$

$$Q_2^* = D_{2u} \frac{d^3 w_2}{dx_2^3}\Big|_{x_2=0} \tag{50-d}$$

3 FINITE ELEMENT MODEL

The finite element method was used as the second method to verify analytical solution. A two-dimensional model was created by ANSYS. Element PLANE 183 was chosen to mesh the geometry model. This high order eight-node element has two degrees of freedom at each node, (translation in the nodal x and y directions). External tensile load (0.6kN/mm) was applied to the right edge of Layer 2 and the left edge of this layer was constrained both in x and y directions. The adhesive layer is Epoxy and adherends are made of aluminum with their nominal mechanical properties expressed by table 1. The geometry of joint is reported by table 2. Figure 7 shows the meshed FEM model.

	E(GPa)	ν
Adherends	69	0.3
Adhesive	3	0.35

Table 1: Mechanical properties of the adherend and adhesive.

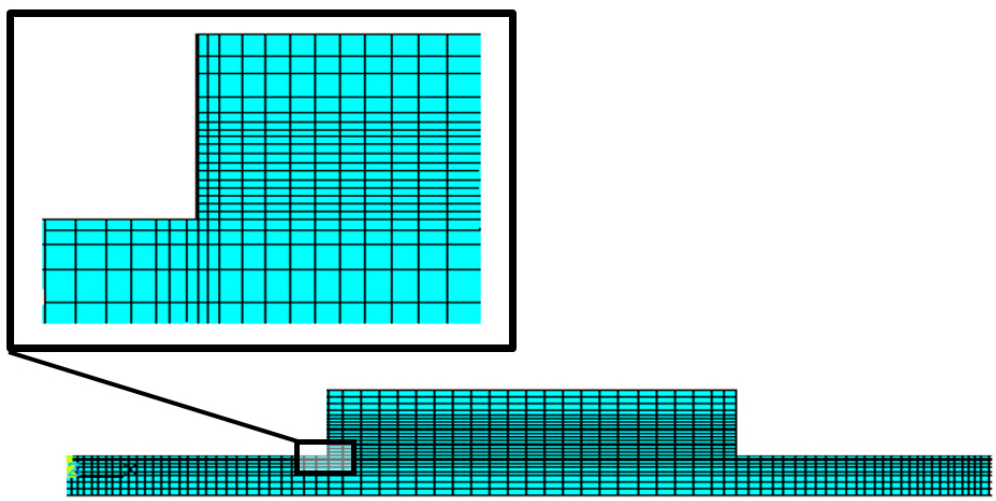

Figure 7: FEM model of a stiffened joint.

t3	0.2
t1	2
t2	2
l	10

Table 2: Geometry details of the model (mm).

4 RESULTS AND DISCUSSION

Derived analytical equations showed that geometry, material properties and load condition affect shear and peel stress distribution along the joint length. These effects are studied in this part beside comparisons of solution methods employed in the article.

4.1 Stiffened Joint

Peeling and shear stress in a stiffened joint are shown in Figure 8 and Figure 9. Results of numerical and analytical method for stress distribution can be compared in the Figures.

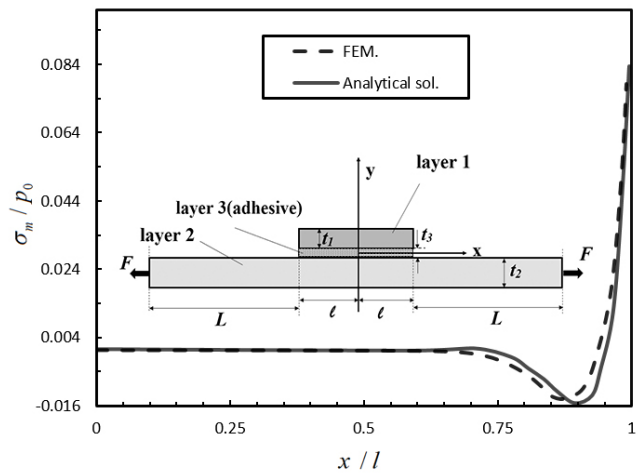

Figure 8: Peeling stress $\frac{\sigma_m}{p_0}$ distribution in overlap region of the stiffened joint.

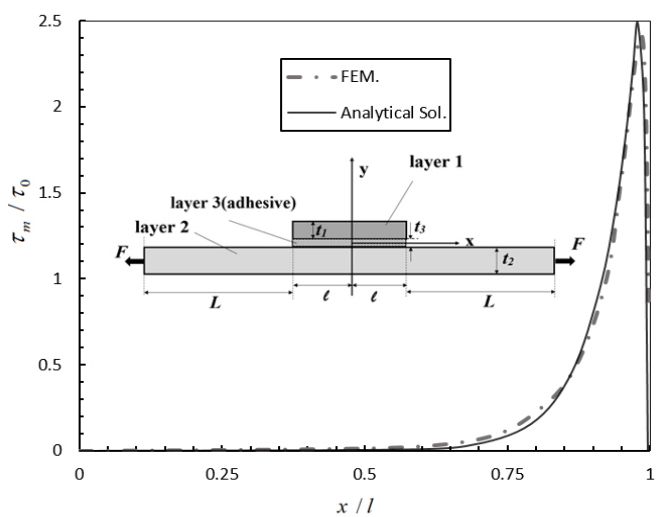

Figure 9: Shear stress $\frac{\tau_m}{\tau_0}$ distribution in overlap region of the stiffened joint.

Figure 8 indicates that peak peeling stress $\frac{\sigma_m}{p_0}$ is at both ends of overlap length. This type of stress is in its minimum value at the middle point of the joint where $x=0$ .Peak shear stress $\frac{\tau_m}{\tau_0}$ occurs at a point near two ends of overlap length as Figure 9 shows. Figures 10 and 11 depict peeling stress distribution between the adhesive and layer 1, σ_{3y}^{u} and the adhesive and layer 2, σ_{3y}^{l}, respectively. Comparing Figure 10 and 11 reveals that peak peeling stress between layer 2 and adhesive is much more than peak peeling stress between the adhesive layer and layer 1. Values of σ_{3y}^{u} and σ_{3y}^{l} are zero except their severe gradient at 12% of both overlap length ends. Except for the end regions of overlap length, FEM results shows good agreement with analytical results. Simplifications due to the applied assumptions may have a role in the incompatibility of results in the end regions.

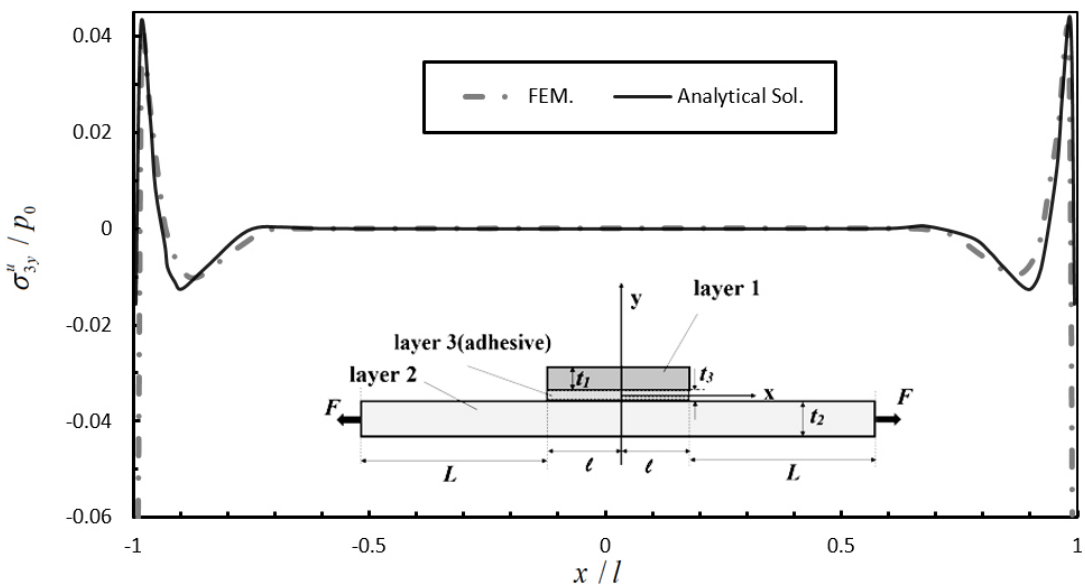

Figure 10: peeling stress distribution between the adhesive and layer 1 in the stiffened joint.

4.2 Single Strap Joint

Figure 12 shows peeling stress distribution in the middle of adhesive layer of the single strap joint. Pay attention to the coordinate axis, where $x=0$. Figure 12 shows that the stress is near zero along the vast length of joint in the middle of adhesive and its peak is at the end of lower adherend by the centerline of joint.

Shear stress distribution in the adhesive layer (in its middle of thickness) along the overlap is depicted in Figure 13.

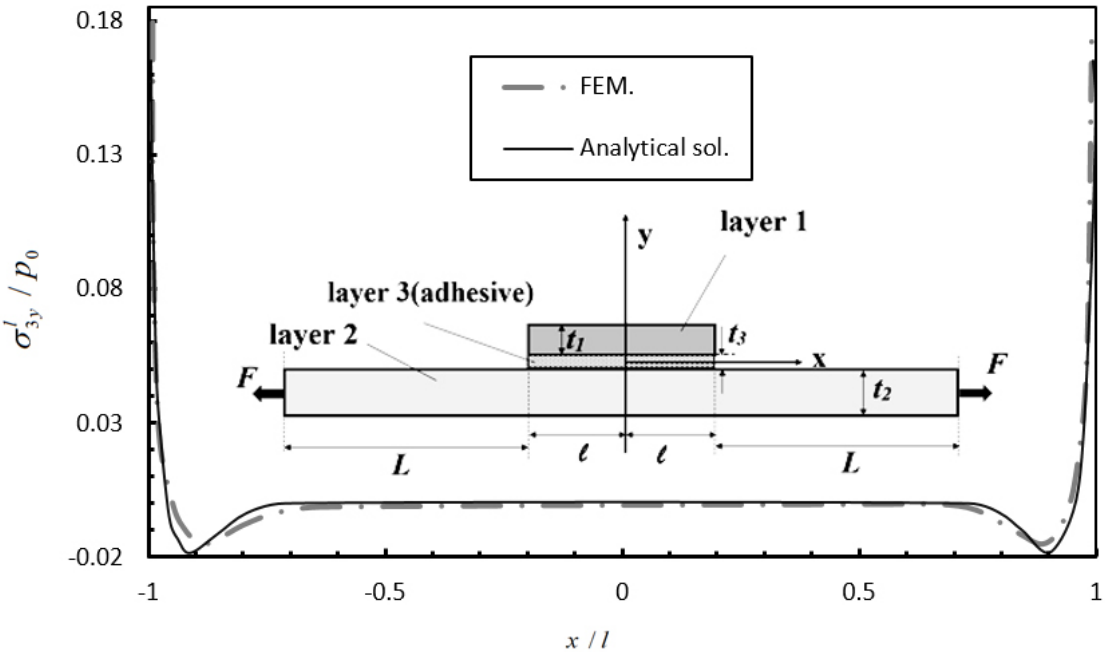

Figure 11: peeling stress distribution between the adhesive and layer 2 in the stiffened joint.

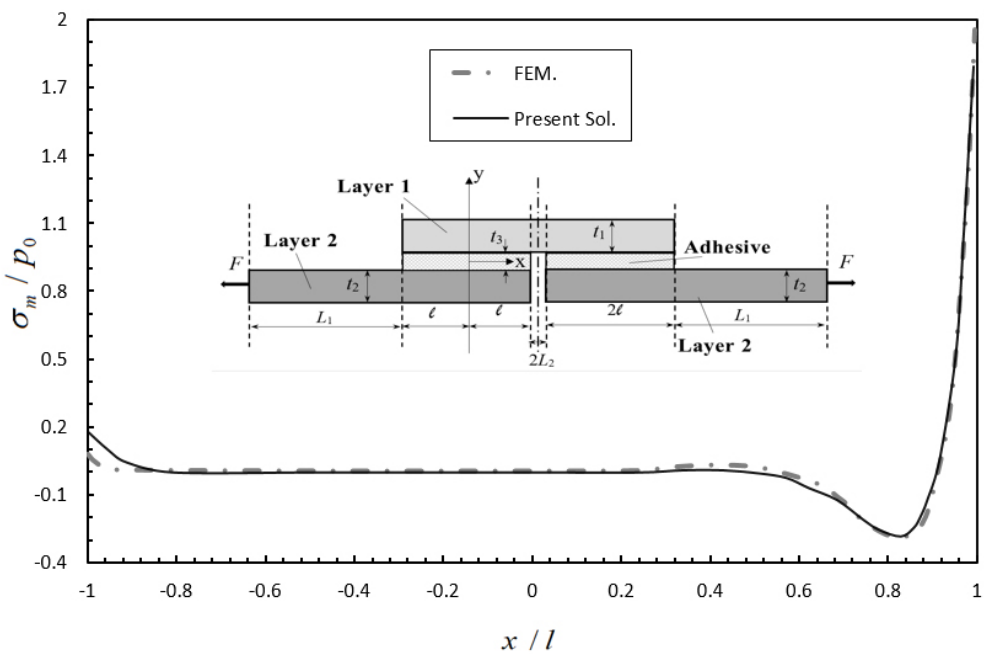

Figure 12: peeling stress distribution in the middle of adhesive layer in stiffened join.

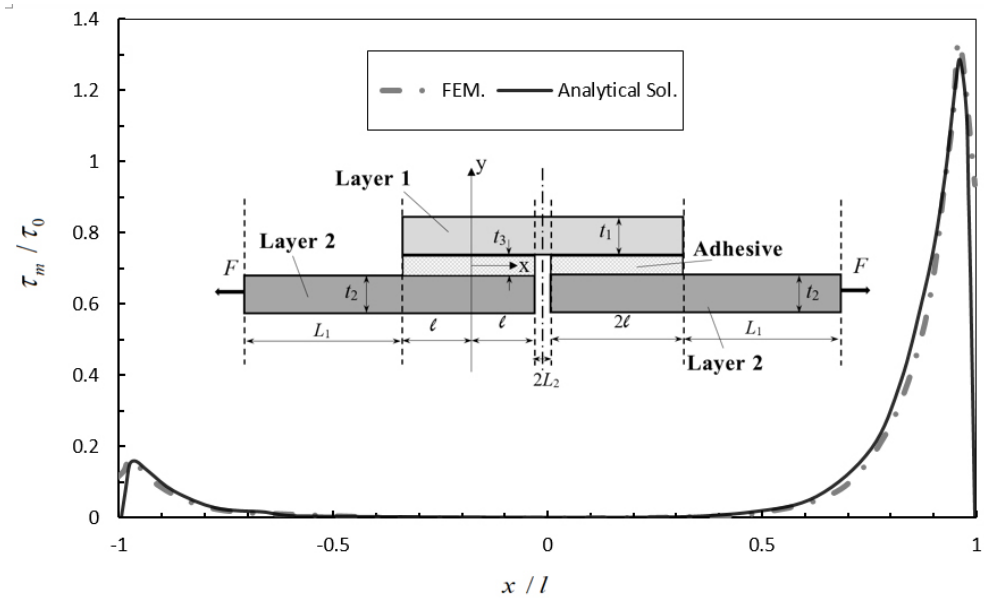

Figure 13: shear stress distribution in the middle of adhesive layer in stiffened join.

Shear stress distribution in Figure 13 declares peak of shear stress is near the internal edge of layer 2. Its value is about zero in along the 75% of overlap length. Shear stress at the left edge of adhesive is about 12% of the peak. Results show that two methods of solution are in good agreement but FEM is more conservative in estimating of maximum stress. Figures 14 and 15 depict peeling stress distribution between the adhesive and layer 1, σ_{3y}^{u} and the adhesive and layer 2, σ_{3y}^{l}, respectively.

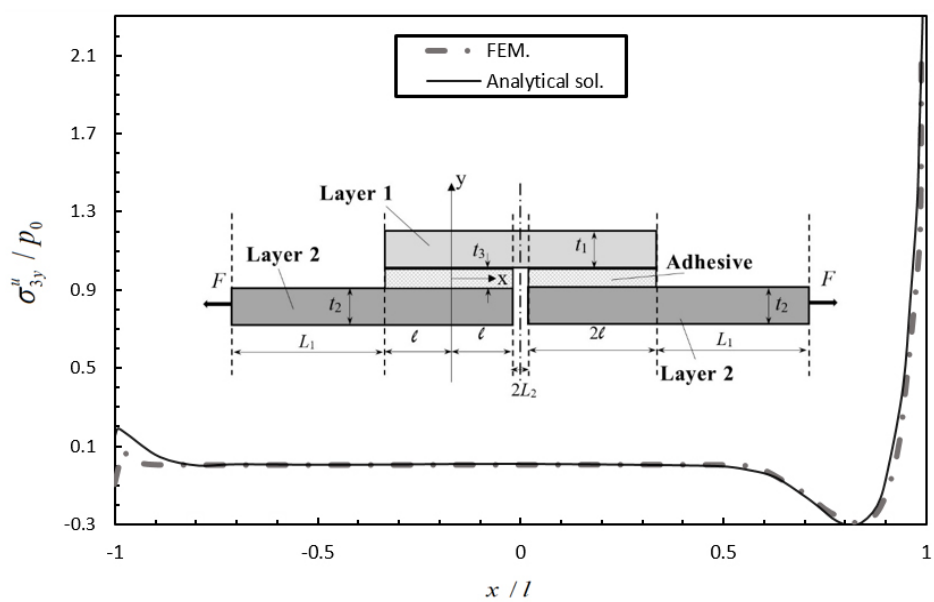

Figure 14: peeling stress distribution between upper adherend and adhesive.

It is observed that peeling stress that is tolerated by the joint between the upper adherend and adhesive is about zero along the overlap except the middle region of joint at the internal edges. In this region the peak stress is occurred. The stress field shown in Figure 15 has a similar shape to depicted field of Figure 14 but it is clear that the peak peeling stress between the upper adherend and adhesive is greater. Peak peeling stress between the lower adherend and adhesive is about 56% of its corresponding value for peeling stress between the upper adherend and adhesive. FEM method agreed analytical solution. In edges some incompatibility are observed and they are considered to be the result of stress concentration.

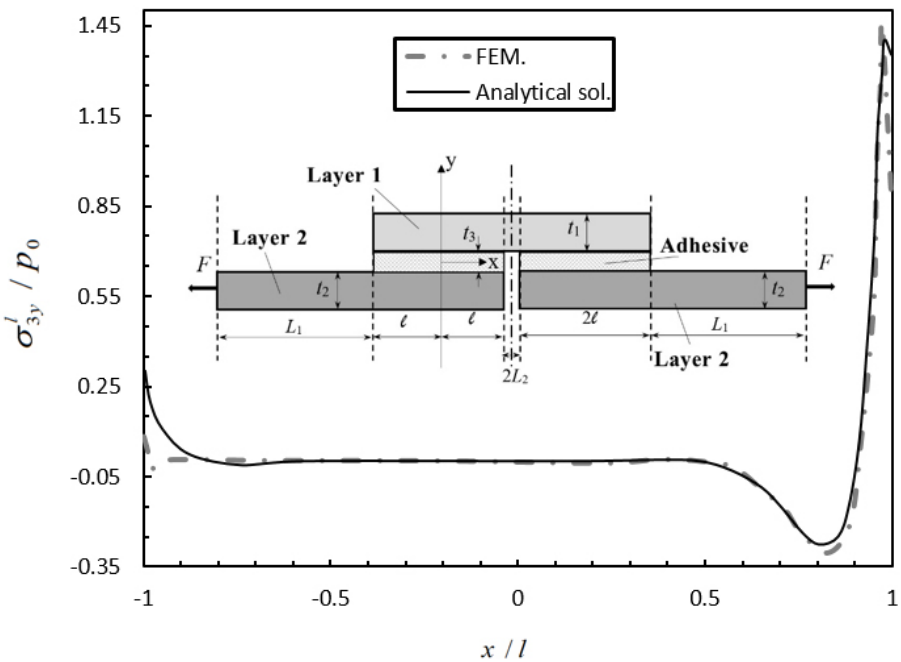

Figure 15: peeling stress distribution between lower adherend and adhesive.

5 CONCLUSION

A stiffened and a single strap joint were studied. The joints were under uniform tensile load and the layers behaved as linear elastic. The analysis were two-dimensional and elasticity theory was used to establish stress-strain and strain-displacement relations. Derived differential equations were solved using appropriate boundary conditions for each joint design. In a stiffened joint peeling stress between adhesive and the lower adherend was much more than its value between the stiffener and adhesive so the critical component in this joint design was lower adherend that tolerated the external load. Peak of shear stress and peeling stress in adhesive occurred at about the middle of the single strap joint near its centerline. Values were negligible in the other points along the length. Peeling stress between adhesive and adherends were greater than its value in the adhesive layer in both of the joints. FEM predicted a more conservative answer for shear and peeling in the single strap joint and was in a good agreement with analytical solutions for both of the joints. Finally

external edges in the stiffened joint and internal edges in the single strap joint were observed as critical locations in designs.

References

Chun, H. (1999). Stress analysis of adhesively-bonded single-lap joints, J. of Composite Structure 47: 673-678.

Ghoddous, B., Shishesaz, M. (2016). Investigation on Void Effect on Shear Stress Field in Bonded Stepped-Lap Joint, J. of Latin American Journal of Solids and Structures 13: 331-343.

Karachalios, E.F., Adams, R.D., Da Silva, L.F.M. (2013). Strength of single lap joints with artificial defects, J. of Adhesion and adhesive 45: 69-76.

Li, G., Sullivan, L.P. (1999). Thring RW. Nonlinear finite element analysis of stress and strain distributions across the adhesive thickness in composite single-lap joints, J. of Comp. Struct. 46: 395–403.

Lou, Q., Tong, L. (2008). Analytical solutions for adhesive composite joints considering large deflection and transverse shear deformation in adherends, J. of International Journal of Solids and Structures 45: 5914-35.

NASA-CR-112235 NASA Langley contract report. Hart-Smith, L.J., (1973). Adhesive-bonded single-lap joints.

Ojalvo, U., Eidinoff, H.L. (1978). Bond thickness effects upon stresses in single-lap adhesive joints, J. of American Institute of Aeronautics and Astronautics Journal 16: 204-211.

Sawa, T., Liu, J., Nakano, K., Tanaka, J. (2000). A two-dimensional stress analysis of single-lap adhesive joints of dissimilar adherends subjected to tensile loads, J. of Adhesion Science and Technology 14: 43-66.

Shahin, K., Taheri, F. (2009). Deformations in adhesively bonded joints on elastic foundations, J. of Composite Structure 90: 130–140.

Shishesaz, M., Bavi, N. (2012). Shear stress distribution in adhesive layers of a double-lap joint with void or bond separation, J. of Adhesion science and technology: 1-29.

Temiz, S., Adin, H., Sulu, I.Y. (2015). Behaviour of Bi-Adhesive in double-strap joint with embedded patch subjected to bending, J. of Theoretical and Applied Mechanics 45: 83–96.

Vable, M., Reddy, J. (2006). Boundary element analysis of adhesively bonded joints, J. of Adhes. 26: 133–144.

Zhao, B., Lu, Z.H. (2009). A two-dimensional approach of single-lap adhesive bonded joints, J. of Mechanics of Advanced Materials and Structures 16: 130-159.